Arab Journal of Sciences & Research publishing
Issue (2), Volume (1)
September 2015
ISSN: 2518 - 5780

المجلة العربية للعلوم و نشر الأبحاث
Arab Journal of Sciences & Research Publishing
AJSRP

Effect of Organoclay on the Morphology, and Thermal Properties of Polystyrene/Poly (vinyl chloride) Nanocomposites

Jumaa Aseeri **Waffa Mekhamer** **Naser Alandis**

Department of Chemistry || Science College || King Saud University || Riyadh || Saudi Arabia

Abstract : Polystyrene and poly (vinyl chloride) (PS/PVC) were prepared via solvent casting method with different weight ratios of PS/PVC: (100/0, 90/10, 80/20, 10/90 and 0/100) to investigate their miscibility. We have studied the morphology of blend PS90/PVC10 (Pd1) with different content (1, 3, 10 %) of organoclay (MM). Cetylpyridinium chloride (CPC) is used to modify the clay sample after saturating its surface with Na+ ions. Fourier transform infrared (FTIR), X-ray diffraction (XRD), and transmission electron microscopy (TEM) were used to characterize the clay sample before and after modification by CPC. The blend miscibility has been confirmed by FTIR, XRD, differential scanning calorimetry (DSC) studies. The prepared nanocomposites were characterized using FTIR, DSC, TEM and scanning electron microscope (SEM). We observed that MM have a significant effect on improvement the miscibility of PS/PVC blends. The thermal stability of the nanocomposites was measured using thermogravimetric analysis (TGA).

1. Introduction

Polymer blends nanocomposites started to attract attention in order to improve the miscibility between different polymers which are immiscible. In that sense, it was suggested that organoclay could contribute to the compatibility of blends based on immiscible polymers and hence improve their properties (Vaia et al., 2011; Essawy et al., 2004). Basically, for compatibilizing two polymeric, the interfacial tension between the phases needs to be lowered. Furthermore, during the blend processing, and the coalescence of the particles needs to be prevented, on expects organoclay to play both roles with polymer blends. The first attempt for using organoclay as compatibility was demonstrated by Gelfer et al., 2003. The studied the effects of organoclay on the morphology, and on the thermal and rheological properties of PS/PMMA (Gelfer et al., 2003). The preparation of nanocomposites from organoclay can follow various routes including in situ-polymerization, solvent casting and melt compounding (Vermogen et al., 2005; Alexandre et al., 2000). Polystyrene (PS) is an excellent polymer for various uses. Its properties can be modified by different means, for example chemically through copolymerization or physically by blending with different materials. At present, physical modification by blending with other polymers is rapidly assuming an important role. PS has only a fair stability for most uses, as it has a rather low heat resistance.

Again poly (vinyl chloride) (PVC) important polymer is quite susceptible toward heat and it has stimulated many workers to investigate this polymer. The rapid expansion and consumption of PVC is due to lower cost, greater availability, both these polymers have a thermal stability than that PS or PVC alone. Nanoscale fillers, especially organoclay, have recently evoked intense research interests as a novel compatibilizer for several types of immiscible polymer blends. Therefore aim this work, investigate the role of modification Saudi clay by cationic surfactant on two immiscible polymer blends of PS/PVC, and the investigation of the influence of wt % of organoclay on morphological and thermal stability of the PS/PVC/ organoclay and a comparison with unfilled PS/PVC. The miscibility of polymers nanocomposites will be characterized using FTIR, XRD, DSC, TEM, and SEM.

2. Experimental

2.1. Materials

Polystyrene (PS) and poly (vinyl chloride) (PVC) were used as a matrix and were supplied by the Saudi Basic Industries Corporation (SABIC). The brand name for polystyrene is PS125, poly (vinyl chloride) is PVC (67S) and the details of polymers are in Table 1. Raw clay sample (M) was collected from Kholais region north of Jaddah in Saudi Arabia and grind in our laboratory. The chemical composition was determined using X-ray florescence (XRF; see Table 2). The silicate surface is generally hydrophilic and compatible with most polymers. To render the hydrophilic clay surface, they are intercalated with organic cations such as alkylammonium salt by a cations exchanger reaction. Cetylpyridinium chloride (CPC), C21H38ClN, molecular weight (358.01 g/mol) and a purity of 99 %, was used provided by BDH & CO, was used as a surfactant. Tetrahydrofuran (THF), C4H8O, which has a molecular weight of (72.11 g/mol) and a purity of 99.5 % was provided by BDH & CO.

2.2. Preparation Methods

2.2.1. Washing and Saturation of clay sample

The clay fraction of clay (M) with fine particle size was separated by the fractional (Mekhamer, 2010). The separated clay was dispersed in 500 ml of 0.5 mol/L NaCl solution, shaken for 24 h. After the clear supernatant was discarded, the clay was again dispersed in 500 ml 0.5 mol/L solution. This process is repeated five times. The Na saturated clay is then washed with distilled water by centrifuging until the AgNO3 test for chloride shows negative. The clay saturated with Na+ thus obtained was dried at 120 °C for 1 h, and finally it was grind, using a pestle mortar. The saturated clay labeled by Na-M.

2.2.2. Modification of clay sample

The organoclay (MM) was prepared using the ion exchange method. 5 g of Na-M were dispersed in 500 ml of distilled for 24 h at room temperature, using a magnetic stirrer. Aqueous solution of CPC was prepared by dissolution of 1.24 g CPC in 100 ml of distilled water. The concentration of CPC solution equivalent to 0.5 CEC of clay sample. The solution of CPC was added gradually under stirring to the dispersion of Na-M for further 12 h stirring. The cation exchange reaction occurs rapidly, and exchange clay was filtered and washed with distilled water until no chloride ion was detected with 0.1 AgNO3 solutions. The resulting organoclay (MM) was dried 60 °C for 24 h under vacuum. Finally, the resulting material was grind using a pestle mortar to obtain a fine powder MM (Calderon et al., 2008).

2.2.3. Preparation of polymer blends (PS/PVC)

A series of polymer blends of PS and PVC were prepared using solvent THF. Polymer solution were prepared by dissolving PS/PVC in various weight ratios (100/0, 90/10, 80/20, 10/90, 0/100) in 20 ml of THF. The solution were mixed at temperature 40-45 °C and stirred for 18 h. Polymer solution of PS and PVC were sonicated in ultrasonic for 0.5 h. The mixture was casting in to petri dishes and allowing the THF to evaporate (Ahmad et al., 2007; Imren, 2010; Kanwal et al., 2008).

2.2.4. Preparation of Pd1/MM nanocomposites

After characterization the above polymer blends, the Pd1 was chosen to study the effect of MM content on the properties of the polymer blend. These blends were prepared at different MM content 1, 3, 10 wt % of MM. In 100 ml beaker were placed a certain mass of MM was added to 10 ml THF. This suspension was stirred magnetically for 1h at room temperature. Then, the Pd1 added to this suspension. The mixture was stirred magnetically for 6 h heating at 40-45 °C then sonicated for 0.5 h. The mixture was casting in to petri dishes with the size of 100*20 mm and allowing the THF to evaporate. The film was removed from the glass plate after 24 h at room temperature. The symbols code of Pd1nanocom-posites prepared at wt % of MM are shown in Table 3.

2.3. Characterization and Measurements

The structure of Na-M, MM powder, polymer blends, and the prepared nanocomposite films were investigated using Fourier-transform infrared (FTIR) spectroscopy. The structure of nanocomposites were monitored using X-ray diffraction (XRD), PAN1Ytical x pert PRO x-ray diffractometer (Holland), and intensity data were collected in the 2θ rang of 3° to 50° with target is CuKα. Wavelength (λ=1.54 Å) source operated at a generator tension of 45 KV and a generator current of 40 mA. Differential Scanning Calorimetry

(DSC) tests of Pd1/MM nanocomposites at different wt % of MM were carried out sing (a TA instruments SDT2960 Simultaneous DSC analyzer). Samples were heated from 25 °C to 200 °C at a scanning rate of 10°C/min under nitrogen flow. Transmission electron microscopy (TEM) images were recorded to investigate the morphology and inner stricter of Pd1/MM nanocomposites samples. TEM images were recorded on a JEOL JSM-6060LV transmission electron microscope. TEM is at an accelerating voltage of 100 KV. For TEM observation, small drops of dilute suspension of 0.1 g of the clays (Na-M and MM) in 5 cm3 of doubly distilled water were placed on copper mesh grids which had been coated with a thin carbon film were air—dried then briefly prior to insertion into the insertion in to instrument. The samples of nanocomposites film were microtomed at room temperature with a diamond knife using in order to obtain 80 nm thick sections, were transferred from water on to copper mesh grids. Phase morphologies were investigated by SEM using a JEOL JSM-6360LV scanning electron microscope. The prepared nanocomposites films were coated with a layer of gold. Thermodegradation of the Pd1/MM nanocomposites were determined using thermogravimetric analysis (TGA) by a Mettler TG-SO instrument. The heating rate was 10 °C/ min under nitrogen flow, over temperature range from 50 °C to 1000 °C.

TABLE 1: Product data for Polymers.

Sample	Mn (gmol-1)	Mwt (gmol-1)	Tg (°C)	Type of polymerization
PS 125	143,000	259,000	89.33	Mass polymerization
PVC 67S	59,000	160,000	84.61	Suspension polymerization

TABLE 2: The chemical composition of raw clay sample.

SiO2	Al2O3	Fe2O3	CaO	MgO	Na2O	K2O	TiO2	Impurities
70.30%	15%	7.75%	2.30%	1.45%	1.20%	0.30%	0.30%	0.10 wt. %

TABLE 3: The symbols cod of Pd1/MM nanocomposites.

Wt % of MM	1 %	3 %	10 %
Pd1/MM	Pd1/1MM	Pd1/3MM	Pd1/10MM

3. Results and Discussion

3.1. FTIR spectroscopy.

3.1.1. FTIR spectra of the Na-M and MM

The FTIR spectra for Na-M and MM are illustrated in Fig. 1 and Table 4. The FTIR of Na-M spectrum indicates that dominant mineral phase in this clay. The bands at 3697 cm-1 and 3625 cm-1 are

due to -OH band stretching for Si-OH and Al-OH, respectively. The broad band centered near 3430 cm-1 is due to -OH stretching band for interlayer water. The absorption peaks in the region of 1636 cm-1 in the FTIR spectra of Na-M is attributed to -OH bending mode in water (adsorbed water). The peak at 1033 cm-1 is attributed to Si-O stretching (in plane) vibration for layered silicates. The IR peak at 915 cm-1 is attributed to Al-OH-Al bending vibrations and 693 cm-1 is attributed Si-O stretching of quartz. The characteristic peak at 527 cm-1 is due to Al-O-Si bending and Si-O-Si bending at around 467 cm-1 (Apatei et al., 2006). The FTIR spectrum of MM is illustrated in Fig.1. The structural changes from hydrophilic to hydrophobic character (Cervantes-Uc et al., 2007; Onal et al., 2008). Similarly, the bending hydration mode in water (adsorbed water) of the -OH groups are characterized by a broad band at 1636 cm-1. This band shifted to 1638 cm-1in the FTIR spectrum of the MM sample, indicating intercalation of surfactant molecules between the silica layers in MM. The broad band observed at 3430 cm-1 is due to –OH stretching band for interlayer water. This band shifted to 3431 cm-1 in MM. The asymmetric and symmetric stretching vibrations of C-H groups belonging to CPC molecules were sharp peaks at 2915 cm-1 and 2850 cm-1 in the FTIR spectrum of the CPC sample were shifts to the 2927 cm-1 and 2853 cm-1 in MM, indicating intermolecular attractions between adjacent alkyl chains of CPC in Na- M galleries (Tzavalas et al., 2009; Ma et al., 2010). The small peak appears at 693 cm-1 is attributed Si-O stretching of quartz shifted to 686 cm-1 in MM. All of these shifts refer to the organophilic modification of the Na-M by CPC (Akyuz et al., 2006; Cole, 2008; Onal et al., 2008; Li et al., 2008).

3.1.2. FTIR spectra of the PS/PVC

The FTIR of PS, PVC, and PS/PVC blends samples were recorded in the region from 400-4000 cm-1, Fig. 2 show the FTIR spectra of PS and PVC and PS/ PVC samples. The IR spectrum of PS showed absorption bands at 3028 cm-1 and 2853 cm-1 corresponding to aromatic and aliphatic C-H stretching, respectively. The C-H stretching vibrations of ring hydrogen's are seen from 3060 cm-1 and 2922 cm-1. The C-H deformation vibration band of benzene ring hydrogen's (5 adjacent hydrogen's) appeared at (1945 cm-1, to 1669cm-1. The peak at 1600 cm-1 is assigned to aromatic C=C stretching. The peak at 1449 cm-1 is for CH2 bending in plane. Peaks at 1069 cm-1and 1028 cm-1 for C-C stretching , at 755 cm-1 and 699 cm-1 for the C-H aromatic bending vibration (mono substituted aromatic ring) , (Cervantes-Uc et al., 2007).

TABLE 4: FTIR assignment of the Na-M and MM.

Assignments Na-M cm-1		MM cm-1
Si-OH Stretching	3697	3697
C-H stretching vibrations of ring pyridinum hydrogen's in (CPC)	-	3653
Al-OH Stretching	3625	3627

Assignments Na-M cm-1		MM cm-1
-OH stretching band for inter layer water hydration	3430	3431
Asymmetric stretching of the CH2 (in CPC)	-	2927
symmetric stretching of the CH2 (in CPC)	-	2853
-OH bending hydration mode in water (adsorbed water)	1636	1638
Si-O stretching (in plane) vibration	1033	1033
Al-OH-Al bending in plane	915	915
Si-O stretching of quartz	693	686
Al-O-Si bending out plane	527	526
Si-O-Si bending	467	465

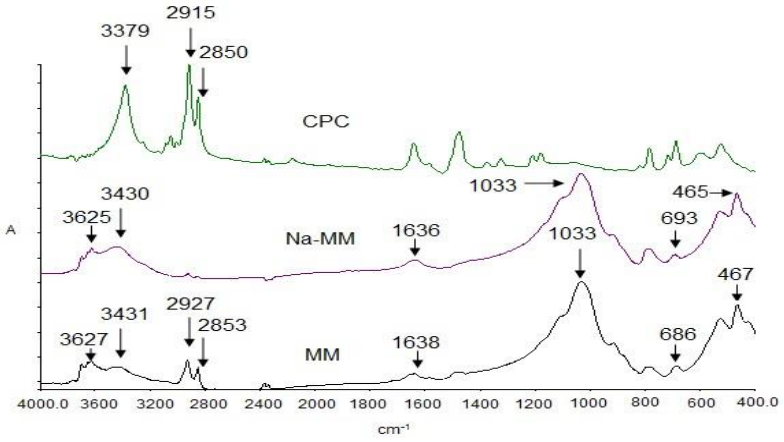

Fig. 1. FTIR spectra of CPC, Na-M and MM.

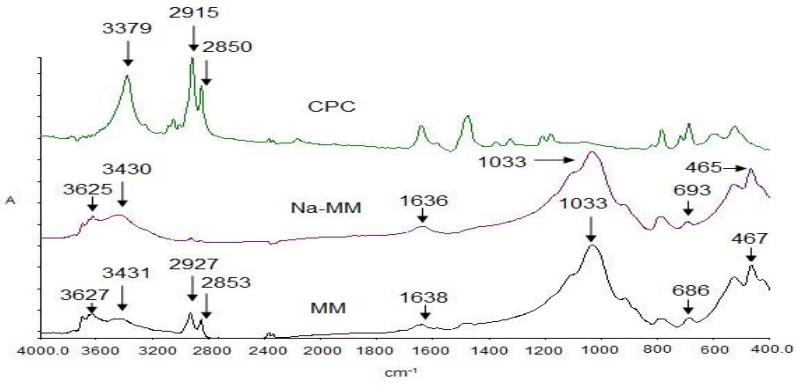

Fig. 2. FTIR spectra of PS/PVC with different content of PVC.

FTIR spectrum of PVC shows peaks at 2972 cm-1, 2913cm-1, 2865 cm-1, 2865 cm-1 , 692 cm-1, 638 cm-1and 618 cm-1 are for C-H of CHCl, C-H of CH2 and C-Cl stretching, respectively, while peaks at

1430 cm-1, 1330 cm-1 and 1252 cm-1 are for CH2 and C-H of CHCl bending in the plane, respectively. The peaks at 1065 cm-1 and 963 cm-1 are for C-C stretching (Kanwal et al., 2008; Khan et al., 2008). For the PS/PVC blends spectra, the peaks corresponding of pure PVC and PS from the 1945 cm-1 to 1430 cm- 1 were appeared in the blend without change in their position. Also there is a considerable different between the spectrum of the blend compared to the spectrum of pure PVC and PS from the 1945 cm-1 to 1430 cm-1were appeared in the blend without change in their position. Also there is a considerable different between the spectrum of the blend compared to the spectrum of pure PVC and PS at the range of 2922 cm-1 to 2864 cm-1 and 1068 cm-1 to 638 cm-1. The FTIR results attribute to probability interaction between the two polymers and formation of physical blend (Kaniappan et al., 2011). On other hand (Kanwal et al., 2008), they determined the physical interaction the two polymers PVC and PS by FTIR.

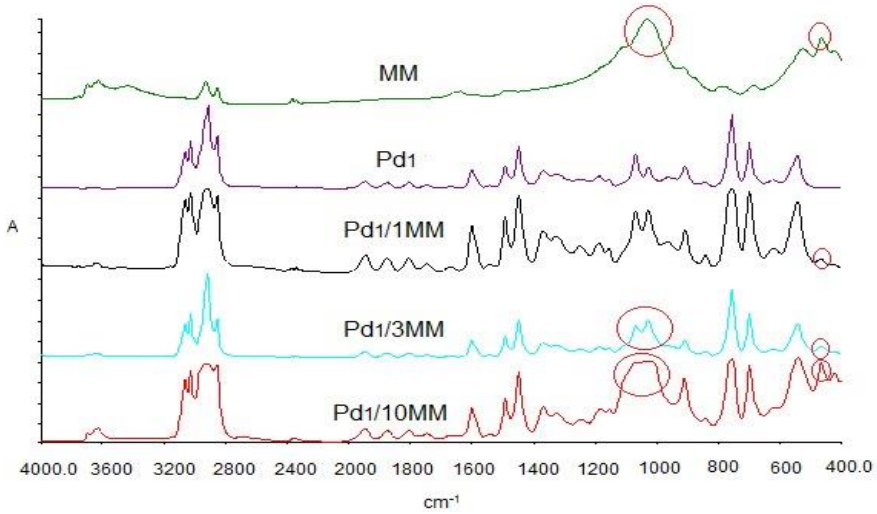

Fig. 3. FTIR spectra of Pd1/MM nanocomposites.

3.1.3. FTIR spectra of Pd1/MM nanocomposites

The FTIR spectra of the Pd1/MM nanocomposites were recorded in region from 400- 4000 cm-1, as shown in Fig.3. The FTIR spectra clearly exhibit the characteristic bands attributable to both the Pd1and MM. This result attributed to the polymer intercalation to the host's layer of the clay by the secondary valence forces to form the Pd1/MM nanocomposites. By comparing the spectrum Pd1 with the spectrum of Pd1/MM nanocomposites, the band at 465 cm-1 which is correspond to Si-O bending vibration of MM was observed. These bands indicate the existence of MM in Pd1/MM nanocomposites. The observation band at 1027 cm-1 is for C-C stretching the Pd1, this peak broaden band when the wt % of MM increase in the nanocomposites,

related to the interaction between organoclay, Pd1 in nanocomposites indicated the insertion Pd between the layers of the MM (Gong et al., 2004; Sain et al., 2011; Bahrami et al., 2011) 3.2. XRD analysis

3.2.1. X-ray of Na- M and MM Fig. 4 shows the XRD patterns of M, Na-M and MM. Upon intercalation of CPC, the basal spacing is increased as expected depending on the surfactant concentrations. The d spacing (001) of MM (Fig. 4) are observed at lower angle compared to Na-M. The d-spacing 12.562 Å (2θ = 7.036°) for Na-M increased to 22.891 Å (2θ = 3.86°) for MM. This demonstrates that baseline spacing (d001, i.e., inter gallery distance) of the layered silicates obtained via the Bragg equation increased due to the exchange of the interlayer sodium by cations CP+ ions. The increasing in baseline spacing after intercalation (Fig.4) provided evidence to support the exchange of the interlayer sodium by cations CP+ ions. Table 5 clearly showed the basal spacing Na-M and MM. A proposed mechanism for CPC molecule adsorption in clay is shown in Fig. 5 (Ray et al., 2003; Nuntiya et al., 2008). The illustration demonstrated the relationship between CPC adsorption and the structure of the adsorption layer influenced by the charge distribution of the clay surface. Initially of clay saturated by concentration of CPC less than 0.7 CEC of clay, adsorption nearly takes place by cation exchange (Figure5 a) (Ray et al., 2003). As the CPC concentration approaches the CEC (0.8-1.0 CEC) of clay, the selective intercalation of CPC develops along the silicate layers Fig.5b, causing the non-uniform interlayer swelling (Fig.5a). As CPC concentration increases beyond the CEC (>1.0 CEC) of the clay, CPC adsorption may predominantly occur via hydrophobic bonding, increasing interlayer spacing to ~40 Å (Fig. 5 c,d) (Ray et al., 2003). Therefore in this work, the suggested mechanism of the structural configuration of alkyl chains of CPC between clay layers is paraffin structure arrangement (Nuntiya et al., 2008). 3.2.2. X-ray of the Pd1/MM nanocomposites Fig. 6 show x-ray diffraction patterns of Pd1 and Pd1/MM nanocomposites with different content of MM (1, 3, 10 wt %) weight ratio lading. The XRD pattern of pure PS as shown in (Fig. 6 A) exhibit an amorphous hump of two halos at 2θ=10.200°, 9.0348 Å and 2θ=20.0°, 4.620Å. The first halo may be attributed to the size of the side group which corresponds to an approximately hexagonal ordering of the molecular chains. The second amorphous halo corresponds to van der Waals distances (Bodor, 1991). The characteristic peaks of the MM disappeared in Pd1/MM nanocomposite, while the broad peaks of Pd1 are observed near its original position (2θ=10.200° and 2θ=20.0°). The absence of basal plane peaks of MM in Pd1/MM nanocomposite indicates the delimitation and dispersion of the MM within the Pd1/MM. This suggests that the MM has exfoliated and dispersed in Pd1 matrix.

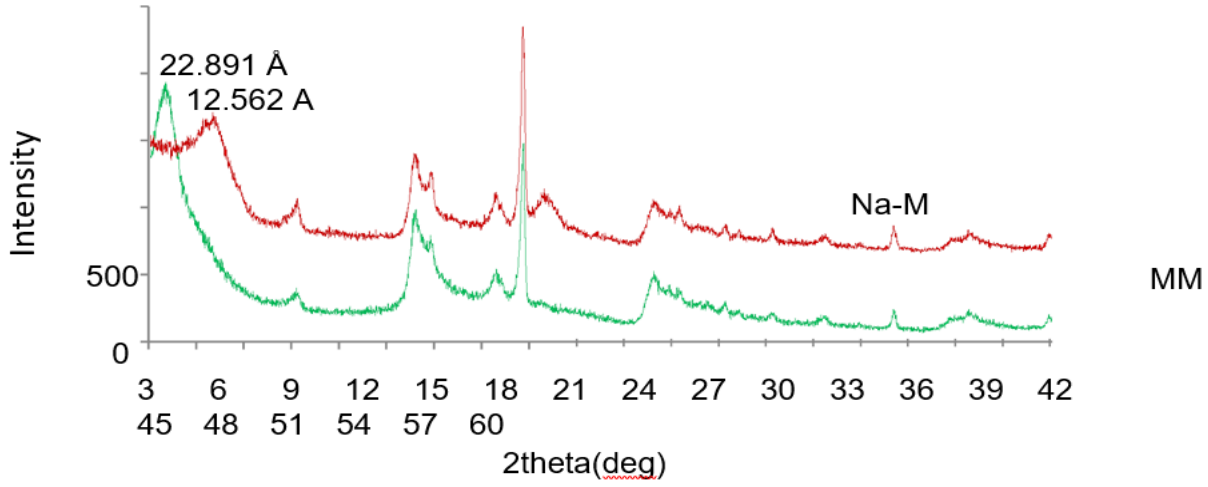

Fig. 4. The XRD patterns of Na-M and MM.

TABLE 5: XRD results of Na-M and MM.

Sample	d 001-spacing (Å)	2θ
Na-M	12.562	7.036
MM	22.891	3.860

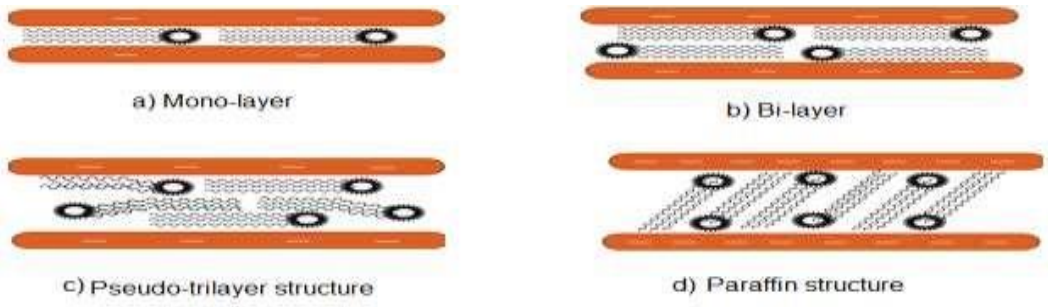

Fig. 5. Potential configuration of interlayer cations.

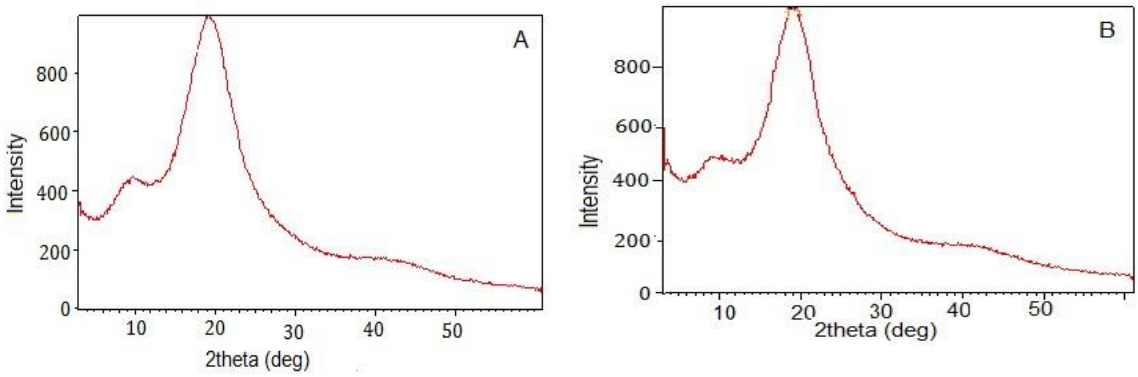

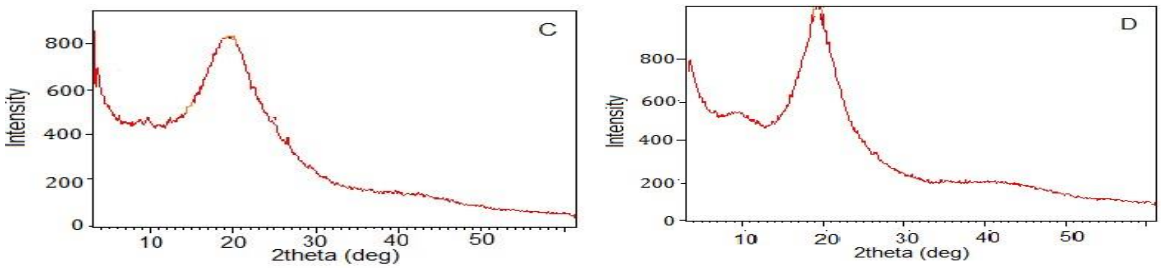

Fig. 6. X-ray diffraction patterns of A) Pd1. B) Pd1/1MM. C) Pd1/3MM. C) Pd1/10MM.

3.3. Differential scanning calorimetry analysis (DSC)

3.3.1. DSC of PS/PVC blends

The measurement of the glass transition temperature (Tg) of a polymer blend is often used as a criterion to determine its miscibility (Pork et al., 2003). DSC has been frequently used for the determination of the glass transition temperature (Tg). The samples were heated from ambient temperature to 200 °C at a heating rate of 10 °C/min under nitrogen flow and were cooled back to room temperature and heated again to 200oC at the same rate. Tg of the samples were measured from the second heating run. Tg's of the samples were determined from the midpoints of the transitions. Fig. 7 shows DSC thermograms of pure PS, PVC and PS/PVC blends. The Tg values for pure PS and pure PVC are about 89.33 °C and 84.61 °C, respectively. A two distinct glass transition temperature (Tg's) was observed for the PS/PVC (90:10) at 91.99 °C and 105oC corresponding to the phases of PS and PVC, showing that phase separation occurs in the polymer blend. While at high content of (PVC in PS–rich phase, 80:20 and PVC-rich 10:90) show a single glass transition temperature Tg (in the temperature range from 89.85°C to 84.30 °C) was identified in the Fig. 7 for PS/PVC (100:0, 80:20, 10:90, 0:100, mass ratio). The results of Tg of PS, PVC and PS/PVC blends are shown in Table 6, a single glass transition temperature Tg is an indication that the synergistic interaction occurs between PS and PVC, also observed when increase PVC content in PS/PVC blends the miscibility of PS/PVC 80:20, 10:90 are better. These results are close to pervious work (Kanwal et al., 2008). Although the blends show a single Tg, is does not definitely mean that mixing has occurred on the molecular scale. While scanning electron microscopy (SEM) and especially transmission electron microscopy (TEM) provides a unique opportunity to illustrate miscibility (Zakarial et al., 2012).

3.3.2. DSC of Pd1/MM nanocomposite

Fig.8 shows the DSC thermograms of Pd1 at different contents of MM (0, 1, 3, 10 wt %). The Tg of Pd1/MM nanocomposites have single glass transition are close to the glass transition of Pd1 as shown in

(Table 7). Organoclay can be useful for compatibilizing polymer blends. Play two roles: first they will decrease the interfacial tension between the two polymeric phases and second they will prevent the coalescence of the microdomains. These results are in agreement with literature (Essawy et al., 2004).

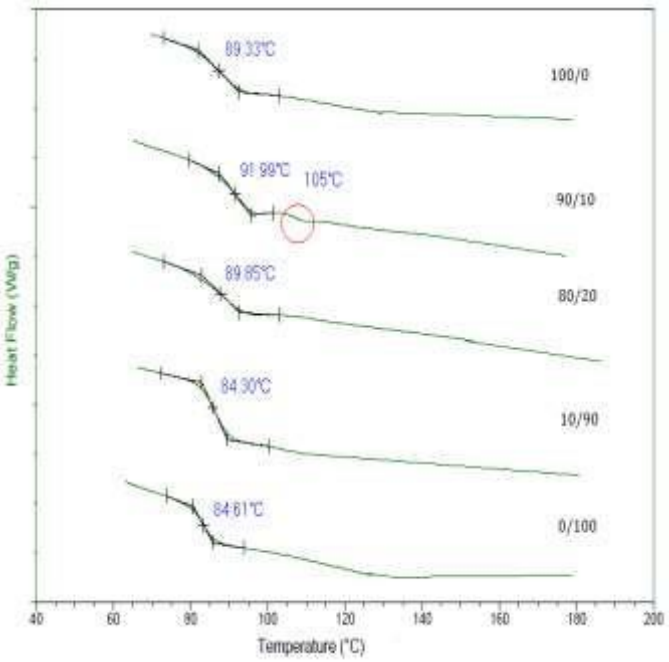

Fig. 7. DSC thermogram of PS/PVC blends

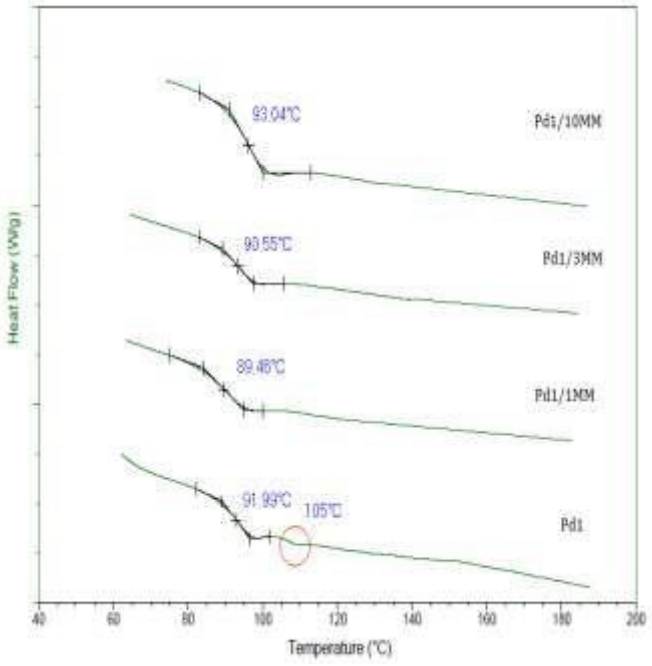

Fig. 8. DSC thermogram of Pd1/MM

TABLE 6: The Tg variation of PS/PVC.

PS/PVC	Glass transition temperature (°C)
100/0 (PS)	89.33
90/10 (Pd1)	91.99 & 105
80/20	89.85
10/90	84.30
0/100 (PVC)	84.61

TABLE 7: The Tg variation of PS/PVC.

PS/PVC	Glass transition temperature (°C)
Pd1	91.99 & 105
Pd1/ 1MM	89.46
Pd1/ 3MM	90.55
Pd1/ 10MM	93.04

3.4. Study the morphology by TEM and SEM.

3.4.1. TEM of Na-M and MM

SEM and TEM provide a unique opportunity to directly visualize nanocomposite morphology. Therefore, the present study aims to take advantage of these techniques to better understand the dispersion mechanisms of layered silicates in polymer blends, as well as to investigate the compatibilization effect of these fillers. The images obtained from TEM analysis of Na-M and MM are shown in (Fig. 9 A-B), respectively. The TEM analysis supports the findings from XRD and FTIR. The Na-M image (Fig. 9 A) shows multilayered silicate platelets are aligned as ordered, parallel and straight lines (dark image). While MM image (Fig. 9 B) shows dispersed silicate platelets (bright image). The bright image due to intercalate of CPC cation between the interlayer distain of clay compared to the Na-M sample. Therefore the layers were almost parallel because of the self-assembled paraffin structure configurations of the CP+ with basal spacing (22.89 Å, as noticed on XRD pattern in (Fig. 4). This result indicates the successful intercalation of the CP+ between clay layers.

3.4.2. TEM and SEM of Pd1/10MM nanocomposite.

In order to gain a better insight into the possible compatilization effect of MM, TEM was used to identify the location of the silicate layers in the polymer blends morphology. Recently, several groups have shown that organoclays can effectively reduce the domain size of polymer blends in several systems (Khatua

et al., 2004; Li et al., 2004). Most of them attribute this effect to the clay acting as a physical barrier. Also the formation of the co- continuous morphology has become important in polymer blends, especially for the development of the polymeric materials with high barrier properties. Fig. (10 A-B) presents the morphology of Pd1, Pd1/10 MM) nanocomposites, prepared by solvent casting, as observed by TEM. In case Pd1 (Fig. 10A), phase separation of nearly spherical PVC droplets suspended in a polymer-rich matrix can be observed. However, when MM added to the Pd1 (Pd1/10MM), the domain size of PVC phase in PS matrix were reduced (Fig. 10 B) compared to the domain size before addition MM (Fig.10 A). This result is attributed to the fact that two immiscible polymer chains can exist together between the intercalated MM; thus, these MM platelets reduced the interfacial tension and enhanced miscibility of the two polymer Pd1 (Gelfer et al., 2003; Khatua et al., 2004). MM platelets with a different orientation can hardly be detected in the high magnification image. The MM platelets are blocked by domain size (PVC phase). On the other hand, (Fig. 11 A-C) represents the SEM images of the pure PS, PVC, Pd1 and Pd1/10MM nanocomposites, respectively. SEM studies indicated that pure PS and PVC, in the films, exist mainly in amorphous state since no crystals in terms of long thin slabs were seen. The SEM image of the Pd1 clearly demonstrated a two-phase (phase separation) compared with pure PS and PVC. The minor phase dispersed as spherical domain phase in polymer rich matrix (Fig. 11C). In addition, the microvoids surrounding the PVC in PS-rich phase droplets indicated weak interfacial adhesion in the blend (Li et al., 2004). Because of the high interfacial tension between the two polymers. Interestingly, addition 10 wt % of MM to the Pd1 resulted in a great decrease in domain phase (PVC phase) (Fig. 11 D). The images (Fig. 11) are in good agreement with those obtained by DSC and TEM.

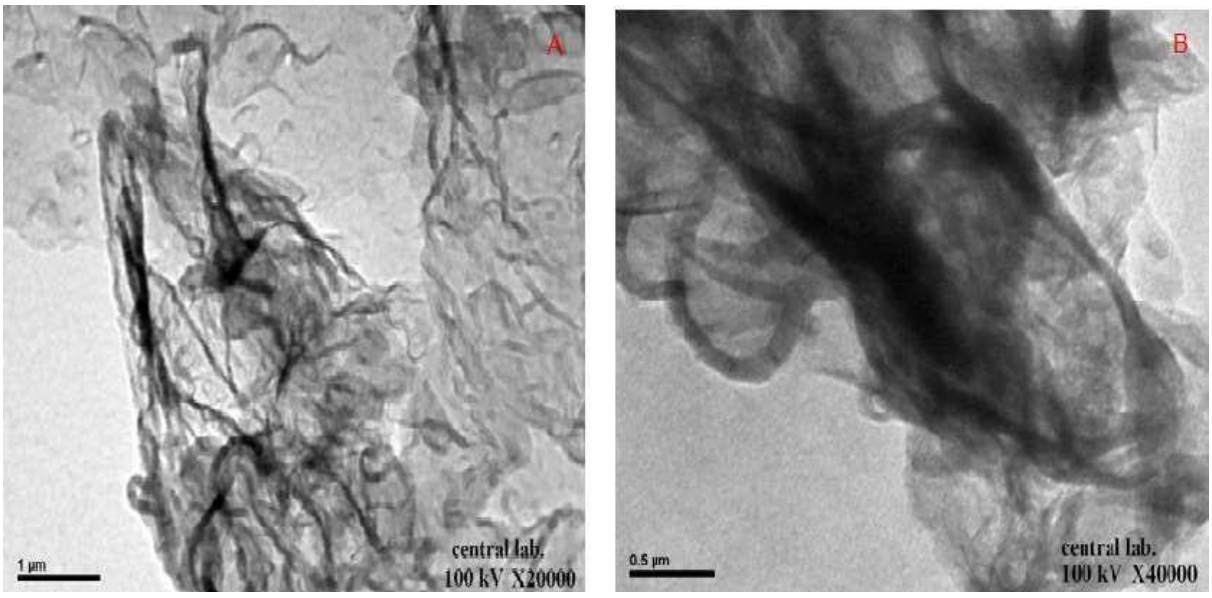

Fig. 9.TEM images of A) Na-M. B) MM.

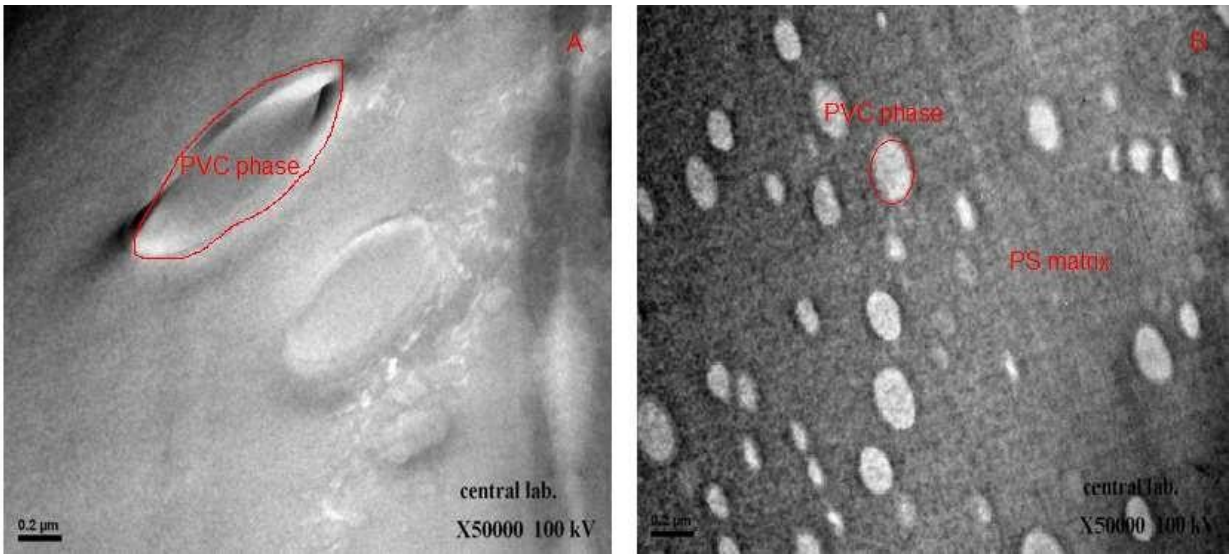

Fig. 10.TEM images of A) Pd1. B) Pd1/10MM.

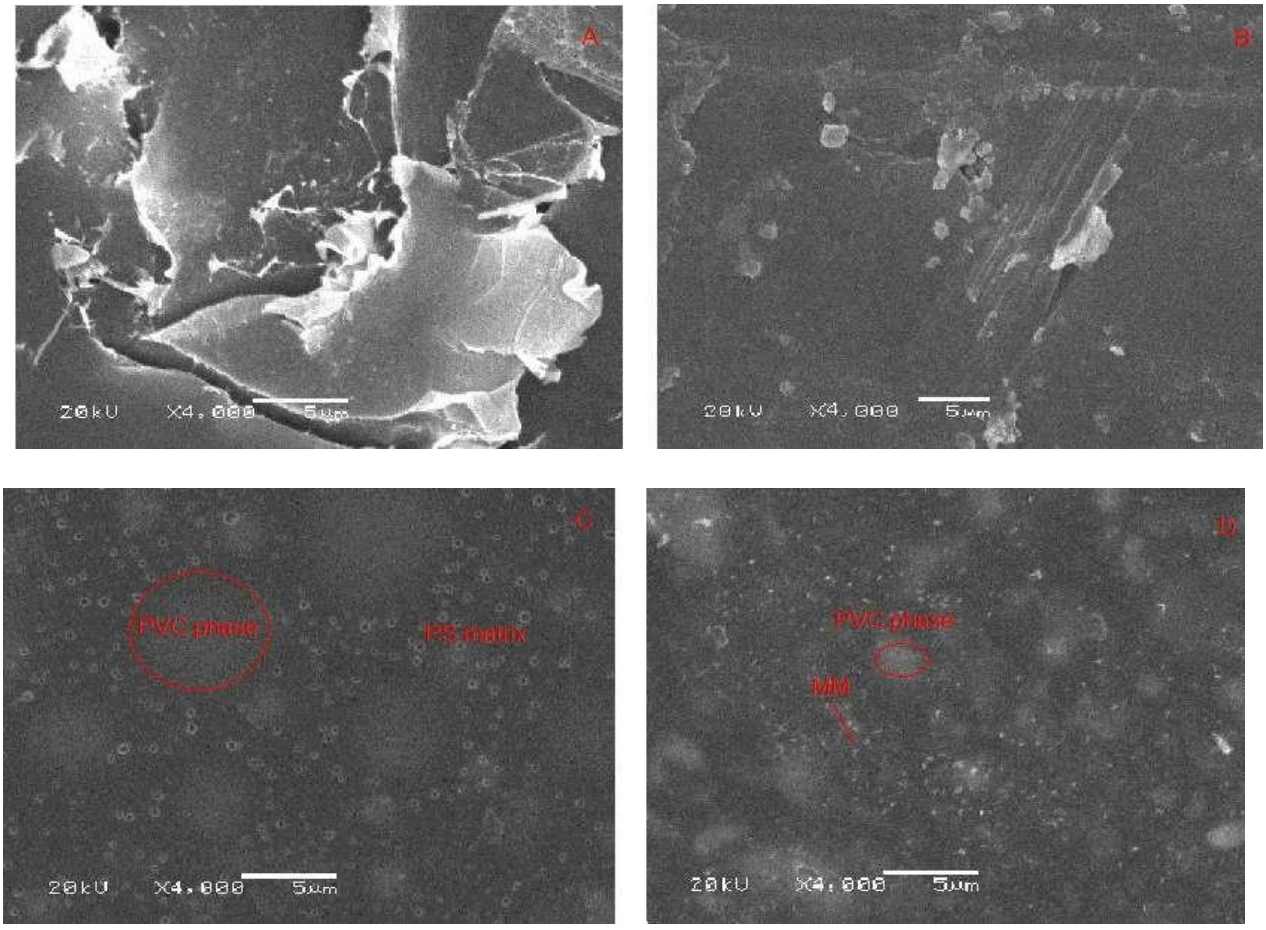

Fig. 11. SEM images of A) pure PS. B) PVC. C) Pd1. D) Pd1/10MM.

3.5. Thermogravimetric analysis (TGA).

3.5.1. TGA of Na-M and MM

Often thermoanalytical studies can lead to new insights into the structure of intercalated clays (Bray et al., 1998). The way in which the mass loss stages occur provides information on the structure of the inserting molecules. The thermogravimetric analysis of Na-M and MM are shown in Fig. 12 A-B. It is noted that the TGA curves and differential thermogravimetric (DTG) of the Na-M has two mass loss stages at between ambient and 100 °C, weight loss 12.14 % and at 464.14°C, weight loss 9 %. These mass loss stages are attributed to desorption of water from the clay surface and the dehydroxylation of the structural units of the clay, respectively.

Four stages of the mass loss are observed for the organoclays (MM). The first stage from the ambient to 100 °C temperature range and is attributed to the desorption of water from MM surface. The second occurs at 293.78 °C, weight loss 23 % (Beall et al., 2004; Xi et al., 2005). This loss attributed to CPC molecules attach to the surface of clay and mainly adhere to surface sites via electrostatic interactions. The third mass loss stage is attributed to the decomposition of intercalated cations (CPC) within the MM interlayer at around 354.89 °C. The fourth stage occurs at 685.06 °C is assigned to the loss of structural hydroxyl groups from within the MM. (Singla et al., 2012; Zeng et al., 2003; Lagaly, 1982). It is noted that the dehydroxylation temperature of the MM (685.06 °C) is higher than Na-M (464.14°C) by 172.16°C. This result is due to two reasons, first, strong electrostatic interaction between negative charge of clay surface and thepositively charged of head group of CPC cation will hold the head group of CPC cation close to the clay surface and secondly the paraffin structure that formed as indicated from XRD result (d001 =22.89 Å).

3.5.1. TGA of PS90/PVC10 (Pd1)

TGA is widely used to investigate thermal decomposition of polymers. These parameters can be used to give a better understanding of the thermal stability of polymer blends. A small weight loss, 5 % occurs in all TGA thermograms which may be due to presence of residual solvent (THF) (Kanwal et al., 2008). Pure PS degrades in nearly one step around 415.97 °C giving mainly styrene monomer, weight loss 92.64 % as shown in (Fig. 13 A). While pure PVC degrades in two steps (Fig. 13 B), the first step attributes to the dehydrochlorination followed by the formation of the conjugated polyene sequences, while the second corresponds to the thermal cracking of the carbonaceous conjugated polyene sequences. The first step occurs, around 297.21°C, weight loss, 60 % while the second step occurs at higher temperature, around 459.06 °C, weight loss 25%. Fig. 13 C shows TGA curves of Pd1, the profile of the Pd1 show two degradation transitions representing the components of the blend. The transition that appeared at higher temperature was

closer to first transition of PVC (301.71 °C in the blend versus 297.2 1 °C for pure PVC) and later one was closer to the pure PS (419.97°C).

3.5.2. TGA of Pd1/MM nanocomposites

The TGA provides important proofs in determining the thermal stability of Pd1/MM nanocomposites with different wt % of MM (1, 3, and 10 %). In general, the weight loss starting at 100°C and ending 900°C (Figure. 14 D-F). Generally the Pd1/MM samples (1, 3, and 10 wt %) of MM exhibit three different types of weight losses: The first step of DTG appears at temperature range of 263.05 -291.83 °C, weight loss 5 % , because of dehydrochlorination for PVC in Pd1. The second step of DTG at temperature range of 420.57 -440.44 °C, weight loss around 87.39 %, due to the thermal degradation of Pd1 chains and the formation of black charred residues. According to the results, the degradation temperature of the Pd1 in nanocomposites has been shifted to higher temperatures compared to Pd1. However, our results agree with (Debnath et al., 2011). Our study suggests that exfoliated polymer/ MM nanocomposites exhibit improved thermal stability. Agglomerated clay particles do not significantly affect the thermal stability of the polymer matrix

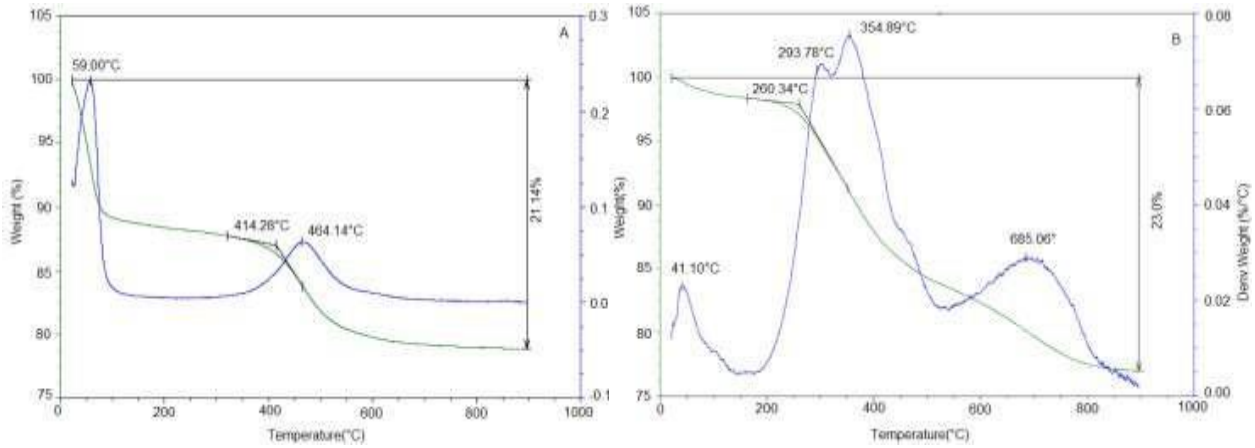

FIG. 12. TGA graphs corresponding DTG graphs of A) Na-M. B) MM.

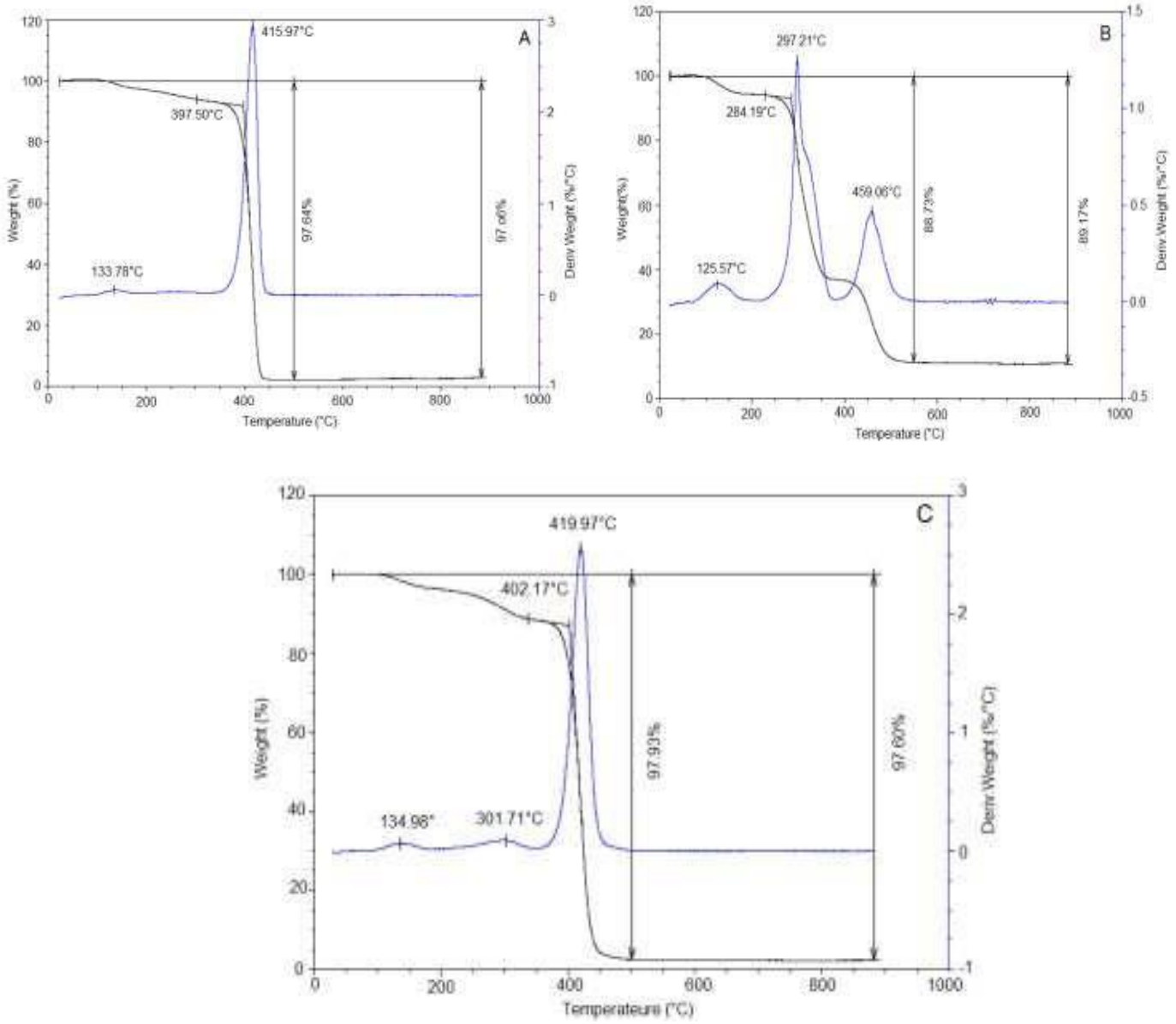

Fig. 13. TGA graphs corresponding DTG graphs of A) PS. B) PVC. C) Pd1

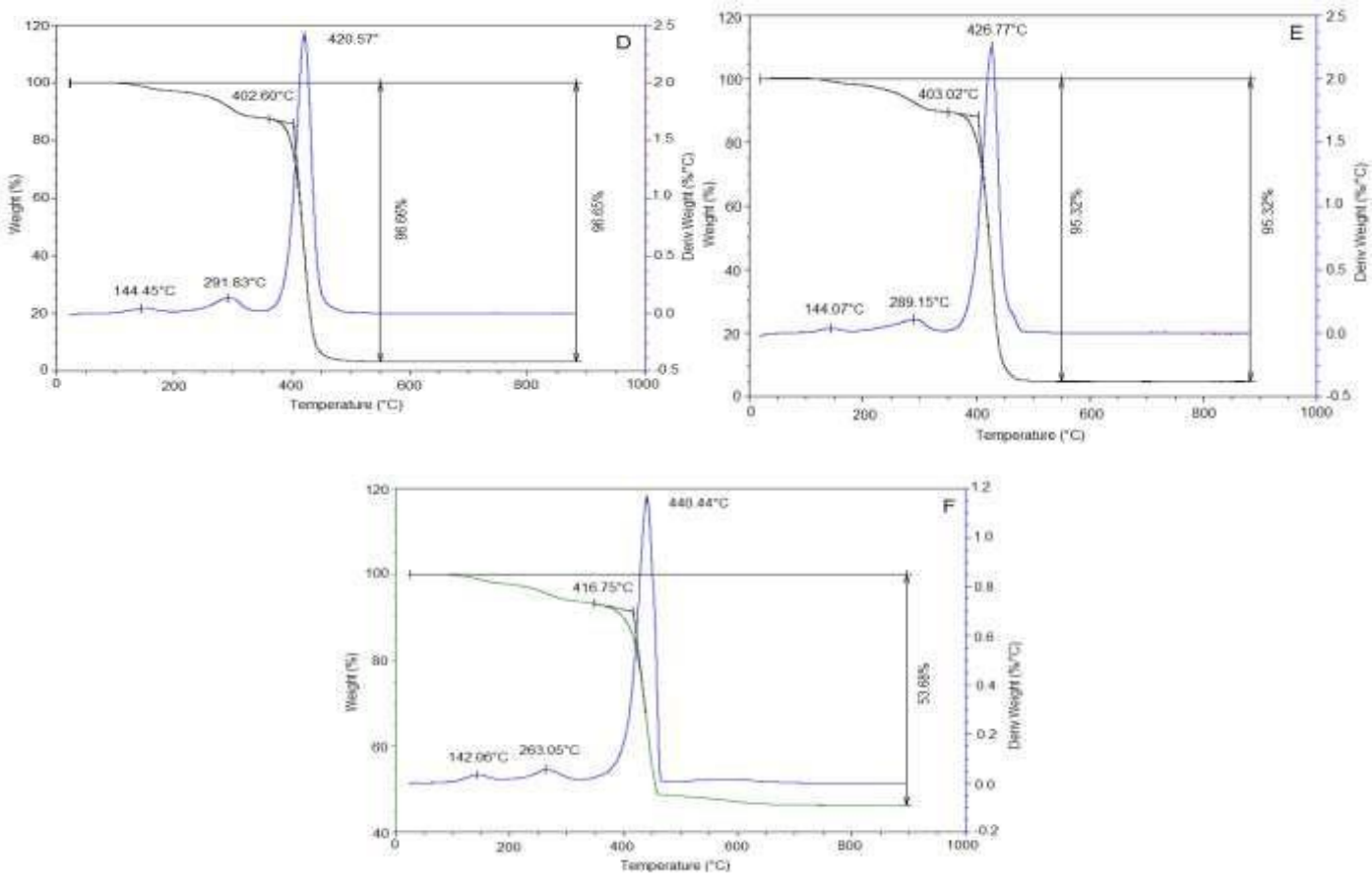

Fig. 14. TGA graphs corresponding DTG graphs of C) Pd1/1MM. E) Pd1/3MM. F) Pd1/10MM.

4. Conclusion

The investigation role of modification Saudi clay by cationic surfactant, CPC on the miscibility of PS/PVC blends. The results of FT-IR, XRD, DSC, TEM, and SEM analyses have shown the following.

1- The FTIR result attribute to interaction probability between the two polymers and formation of physical blend. FTIR spectra confirmed the insertion of Pd1 (PS90/PVC10) between the layers of the MM.

2- The results of XRD show that exfoliated structure were obtained for all Pd1/MM nanocomposites.

3- From DSC, TEM and SEM well correlated together, it was shown that MM have a significant effect on improvement the miscibility of Pd1 blend

Acknowledgment This Project was supported by King Saud University, Deanship of Scientific Research, College of Sciences Research Center.

References

1- Apatei, H. S., Soman, R. C., Bajaj, H. V., Jasra, R., 2006. Nanoclays for polymer nanocomposites, paints, inks, greases and cosmetics formulations, drug devery vehicle and waste water treatment. Bulletin of Materials Science 29 (2), 133-145.

2- Alexandre, M., Dubois, P., 2000. Polymer-layered silicate nanocomposites: preparation, properties and uses of a new class of materials. Materials Science and Engineering 28, 1-63. Akyuz, S., Akyuz, T., 2006. FT-IR spectroscopic investigation of adsorption of 2-, 3- and 4- pyridinecarboxamide on montmorillonite saponite from Anatolia. Vibrational Spectroscopy 42 (2), 387-391.

3- Ahmad, Z., Al-Awadi, N. A., Al-Sagheer, F., 2007. Morphologym thermal stability and visco-elastic properties of polystyrene epoly (vinyl chloride) blends. Polymer Degradation and Stability 92, 1025-1033.

4- Bodor, G., 1991. Structural investigation of polymers, Ellis Horwood Limited Chichester. England, 230-357.

5- Beall, G., Goss, M., 2004. Self - assembly of organic molecules on montmorillonite. Applied

6- Clay Science 27, 179-186.

7- Bahrami, H., Mirzaie, Z., 2012. Polypropylene/ modified nanoclay composite-processing and Dye-ability properties. World Applied Sciences Journal 13(3), 493-501.

8- Bray, H. J., Redfern, S. A., Clark, S. M., 1998. The kinetics of dehydration in Ca- montmorillonite, an in sitiu x-ray diffraction study. Mineralogical Magazie 62, 647-656. Cervantes-Uc, J., Cauich-Rodriguez, J., Vazquez-Torres, H., Garfias-Mesias, L., Paul, D. Thermal degradation of commercially available organoclays studied by TGA-FTIR. Thermochimica Acta 457(457), 92-102.

9- Cole, K. C., 2008. Use of infrared spectroscopy to characterize clay intercalation and exfoliation in polymer nanocomposites. Macromolecules 41(41), 834-843.

10- Calderon, J. U., Kamal, M. B., 2008. Thermally stable phospouium Montmorillonite organoclay. Applied Clay Science40(1-4), 90-98.

11- Dbnath, D. khatua, B. B., 2011.Preparation by suspension polymerization and characterization of polystyrene (PS)-poly(methyl methacrylate) (PMMA) core-shell nanocomposites. Macromolecular Res-erch 19(6), 519-527.

12- Essawy, H., EL-Nashar, D., 2004. The use of montmorillonite as a reinforcing and compatibilizing filler for NBR/SBR rubber blend. Polymer Testing 23 (7), 803-807.

13- Gelfer, M. Y., Song, H. H., Liu, L., Hsiao, B. S., Chu, B., Rafailovich, M., Si, M., Zaitsev, V., 2003. Effects of organoclays on morphology and thermal and rheological properties of polystyyrene and poly (methyl methacrylate) blends. Journal of Polymer Science Part B: Polymer Physics 41(1), 44-54.

14- Gong, F., Feng, M., Zhao, C., Zhang, S., Yang, M., 2004. Thermal properties of poly(vinyl chloride) / montmorillonite nanocomposites. Polymer Degra-dation and Stability, 84(2), 289-294.

15- lmren, D., 2010. Compatibilization of immiscible poly(vinyl chloride) (PVC)/ polystyrene (PS) blends with maleic anhydride-styrene-vinyl acetate terpoly-mer (MASTVA). Journal of Molecular Structure 963, 245-249.